JOURNAL OF CATALYSIS **175,** 328–337 (1998)
ARTICLE NO. CA982019

Kinetics and Intraparticle Diffusion Modelling of a Complex Multistep Reaction: Hydrogenation of Acetophenone over a Rhodium Catalyst

Isabelle Bergault,*[,1] Pierre Fouilloux,* Catherine Joly-Vuillemin,* and Henri Delmas†

*Laboratoire de Génie des Procédés Catalytiques, CNRS, CPE Lyon—BP2077, 43 Bd du 11 Novembre 1918, 69616 Villeurbanne Cedex, FRANCE; and †Laboratoire de Génie Chimique, CNRS, 18 Chemin de la Loge, 31078 Toulouse Cedex, FRANCE

Received October 9, 1997; revised December 8, 1997; accepted January 12, 1998

In a first step the intrinsic kinetics of acetophenone hydrogenation on a Rh/C catalyst was studied in a semi-batch reactor. Tiny catalyst grains of 17 μm in average diameter were used in order to avoid any intraparticle diffusion limitation. Experiments were performed over a wide range of operating conditions and various Langmuir–Hinshelwood kinetic equations were discriminated over the complete conversion range. The model based on nondissociative adsorption of hydrogen and noncompetitive adsorption of the organic species with the gas molecules was found to fit better all the experimental data. The relevance of its optimized parameters was then discussed. In a second step the intraparticle diffusion limitations were also studied in a semi-batch reactor by varying the particle size. Two models based on the complex kinetics previously established were developed, taking into account the catalyst grain size and shape. After an additional adjustment of one of the adsorption constants ratios, they were found to provide a good representation of the data in terms of activity and selectivity.

INTRODUCTION

Three phase catalytic hydrogenations are commonly used in a large number of chemical processes. They are usually carried out in fixed bed reactors wherein gas and liquid are flowing through a bed of large catalyst particles, or in reactors containing a slurry of small catalyst particles suspended in the gas–liquid mixture. The design and scale-up of these multiphasic devices involve many aspects including complex coupled phenomena and require accurate kinetic laws as well as reactant transfer calculations.

Acetophenone hydrogenation has already been chosen by other authors as a model reaction for kinetics studies. On the one hand, it is of industrial relevance because its intermediates and products are used in the pharmaceutical and cosmetic industry. On the other hand, it is a good example of a complex multistep reaction. The reported results (1–8) show clearly the strong dependence of the reaction scheme towards catalyst nature and operating conditions. Most of the kinetic studies reported in the literature concern the selective hydrogenation of acetophenone into phenyl 1-ethanol followed by the hydrogenolysis into ethylbenzene. The studies performed with this complex reaction scheme are often based on oversimple hypotheses as power law kinetics (3, 4, 9–12) and only a few models, based on the more realistic Langmuir–Hinshelwood hypothesis, are available (7, 14, 20). They all suppose that the reaction at the catalyst surface is the rate limiting step. Some authors propose a competitive adsorption of the species but they are not able to choose between a dissociative or nondissociative adsorption of hydrogen because, either they performed their experiments at a constant hydrogen pressure (13), or the agreement between the experimental results and the computed values obtained with the dissociative and nondissociative models is not significantly different (7, 14).

In the present work, experiments were performed over a wide range of operating conditions. Rhodium supported on carbon was chosen as the catalyst and cyclohexane as a nonhydroxylated solvent, in order to hydrogenate the aromatic ring as well as the ketone function. Our aim was, first, to select a suitable kinetic model fitting our experimental data and, second, to discuss the methodology to be followed in the case of a complex reaction scheme. The analysis of the data was based on the complete kinetics, using the whole concentration profiles and the hydrogen consumption versus time all along a given experiment. This method was proved to be more effective than using only initial kinetics (15). The model discrimination and parameter optimization are reported in this paper and the results discussed. The intraparticle diffusion effects were then studied and a model developed in order to predict the reaction rates and selectivities with the large particles used in trickle-bed reactors.

EXPERIMENTAL

The hydrogenation of acetophenone (Aldrich, 99% min) was carried out using cyclohexane (RP Normapur Prolabo 99.5% min) as a solvent and in the presence of a

[1] Corresponding author.

0021-9517/98 $25.00

Rh catalyst supported on coconut shell activated carbon (Degussa, 3% Rh/C, G181 XKB/D). Rh/C was provided as large particles of an average diameter $d_p = 3.37$ mm. A scanning microscope diagram showed that the metal is not uniformly dispersed on the carbon support. The distribution of the metallic crystallites is of eggshell type, the core being free of metal. A catalyst particle tortuosity factor equal to 5, generally considered as an average, was taken. The other characteristic parameters were its density $\rho_s = 2105\ \text{kg} \cdot \text{m}^{-3}$, apparent density $\rho_{app} = 980\ \text{kg} \cdot \text{m}^{-3}$, porosity $\varepsilon_p = 0.53$, and specific surface area $S_{BET} = 870\ \text{m}^2 \cdot \text{g}^{-1}$. To obtain particle samples of uniform size the commercial catalyst was crushed and sieved. The finest particle size ($d_p = 17\ \mu\text{m}$) was used for the intrinsic kinetic study.

Experiments were carried out in a stainless steel agitated semi-batch reactor with a classical manifold for hydrogen supply at constant pressure. Its maximum capacity was 150 cm^3 and its optimum content in volume was 60 to 75 cm^3. Baffles and magnetic agitation provided a good gas–liquid mass transfer. The temperature regulation led to temperature variations less than ±1 K. In each experiment, 0.5 g of catalyst (3% Rh/C, $d_p = 17\ \mu\text{m}$) were charged with 45 g of solvent. Catalyst was pretreated in cyclohexane under hydrogen pressure (1.8 MPa) during 1 h at 368 K. Then, after the operating conditions were attained, acetophenone contained in a reagent supply vessel was introduced into the gas–liquid–solid mixture. The pressure was maintained constant during an experiment by adjusting the hydrogen feed to the consumption by means of a pressure regulator. Liquid samples were withdrawn at regular intervals of time and analysed by gas chromatography, using a polar and capillar column (type BP20) and the data obtained from the experiments were reproducible within ±5%. We used constant hydrogen pressures varying from 0.5 to 4.0 MPa, temperatures from 333 to 373 K and acetophenone initial concentrations from 0.118 to 1.14 mol/liter. For the intraparticle diffusion study, experiments were performed at T = 353 K under $P_{H_2} = 2.5$ MPa, for different particle sizes (17, 50, 100, 500, and 3370 μm). The hydrogenation of pure intermediates like phenyl 1-ethanol or methylcyclohexylketone, was also performed in order to elucidate the reaction scheme.

RESULTS

Kinetics of the Reaction Controlled by Chemical Regime

Reaction Scheme and Conversion Measurements

From the GC analysis, six molecules coming from the hydrogenation of the aromatic ring and/or of the ketone function were identified: methylcyclohexylketone, phenyl-1-ethanol, cyclohexyl-1-ethanol, phenyl-1-ethanol, ethylbenzene, and ethylcyclohexane. Considering the contribution of each compound to the total mass balance, it appears

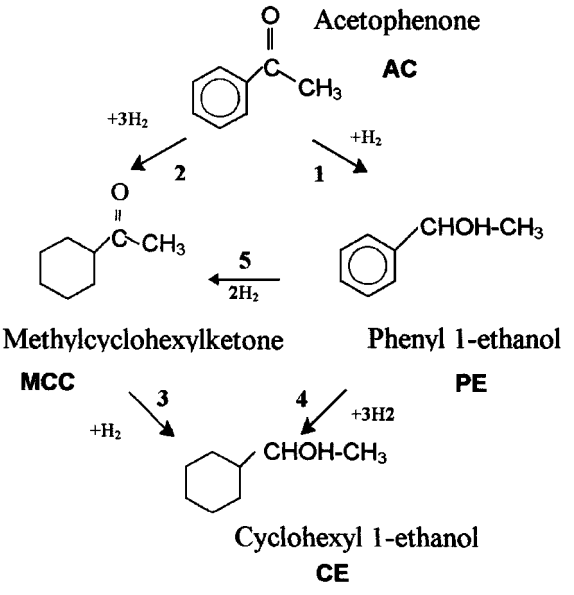

FIG. 1. Reaction scheme of acetophenone hydrogenation on Rh/C catalyst.

that the last two represent only 3%. The simplified reaction scheme of Fig. 1 was then proposed, where we considered only the compounds with significant concentration.

Figures 2 and 3 show typical hydrogen consumption curves and the concentration profiles of reaction products plotted versus time during an experiment. The hydrogen consumption was measured from the pressure loss in a storage vessel and was systematically checked to be in good agreement with the mass balance based on the liquid phase concentrations. From these curves, initial global rates of hydrogenation were measured, with an accuracy of ±10% and used for preliminary discussions on model discrimination. Concentration profiles versus time were required for software determination of kinetic parameters.

Checking the Chemical Regime

In order to determine the intrinsic kinetics of the reaction, it was necessary to ensure that none of the external

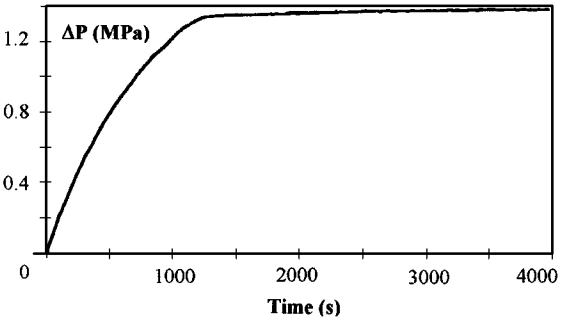

FIG. 2. Hydrogen consumption versus time for $P_{H_2} = 2.5$ MPa, T = 353 K, $m_{cata} = 0.5$ g, and $C^{\circ}_{AC} = 0.6\ \text{mol} \cdot \text{l}^{-1}$.

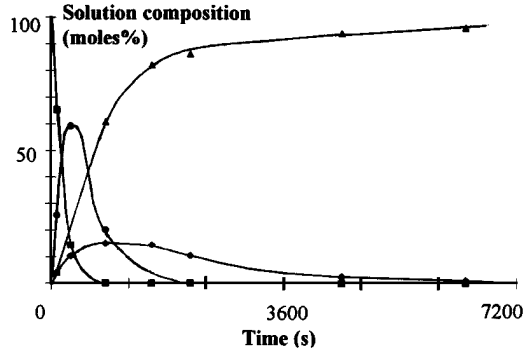

FIG. 3. Concentration profiles versus time for $P_{H_2} = 2.5$ MPa, T = 353 K, $m_{cata} = 0.5$ g, and $C^{\circ}_{AC} = 0.6$ mol·l^{-1}, (■) AC, (◆) MCC, (▲) CE, (●) PE.

or internal mass transfer resistance was limiting in our reaction conditions. For this purpose, gas–liquid and liquid–solid mass transfer, as well as internal diffusion limitations were examined separately.

When gas–liquid mass transfer is totally limiting, the hydrogen consumption becomes independent from the catalyst loading and the hydrogen flux through the gas–liquid interface is expressed as ($k_{G\text{-}L}$, $a_{G\text{-}L}$ gas–liquid mass transfer coefficient and gas–liquid interphase area; V_L liquid volume):

$$\varphi_{G\text{-}L} = k_{G\text{-}L} a_{G\text{-}L} \left(C^{*}_{H_2} - C_{H_2,1}\right) V_L \quad (\text{kmol} \cdot \text{s}^{-1}).$$

The influence of the mass of catalyst on the initial hydrogenation rate was then investigated for the most drastic operating conditions (P_{H_2} = 4 MPa, T = 373 K, C°_{AC} = 0.6 mol/liter). The results, plotted on Fig. 4, show the linear dependence of the initial rate with the catalyst weight, proving that the gas–liquid mass transfer is not limiting.

In order to determine if the liquid–solid mass transfer resistance was limiting, the observed reactants consumption rates (r_{H_2} and r_{AC}) were compared to the minimum transfer rates obtainable in the case of a limiting

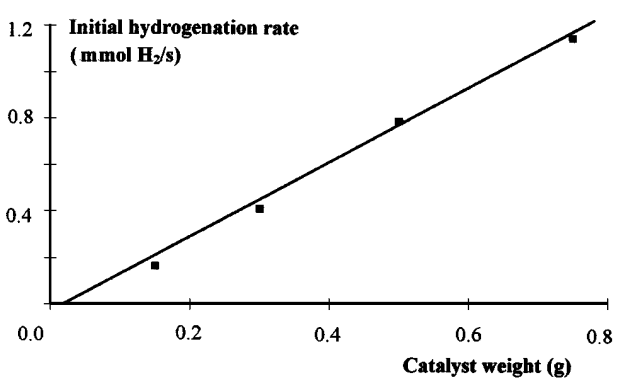

FIG. 4. Initial rate of hydrogenation as a function of catalyst loading; $P_{H_2} = 4$ MPa, T = 373 K, $C^{\circ}_{AC} = 0.6$ mol·l^{-1}.

liquid–solid mass transfer ($\varphi_{L\text{-}S(H_2)} = k_{L\text{-}S} \cdot a_P \cdot C^{*}_{H_2} \cdot V_L$ and $\varphi_{L\text{-}S(AC)} = k_{L\text{-}S} \cdot a_P \cdot C_{AC} \cdot V_L$, expressed in kmol·s^{-1} with $\varphi_{L\text{-}S}$ liquid–solid mass transfer coefficient). The minimum possible value for $k_{L\text{-}S}$ was evaluated, considering that the Sherwood number ($Sh = k_{L\text{-}S} \cdot dp/D_i$) would equal 2 in this case. Molecular diffusivities D_i were estimated by Wilke and Chang's correlation (16). As an example, experimental results and calculations performed at T = 353 K, P_{H_2} = 4 MPa, and $C^{\circ}_{AC} = 0.6$ mol/liter gave

$$r_{H_2} = 0.757\ \text{mmol} \cdot \text{s}^{-1} < \varphi_{L\text{-}S(H_2)} = 9.7\ \text{mmol/s}^{-1}$$

$$r_{AC} = 0.11\ \text{mmol} \cdot \text{s}^{-1} < \varphi_{L\text{-}S(AC)} = 5.93\ \text{mmol/s}^{-1}.$$

So the experimental rates are far lower than those totally limited by liquid–solid mass transfer and cannot be affected by diffusion to the grain surface.

The internal diffusion limitations were experimentally investigated. From experiments carried out for different catalyst particle sizes at T = 353 K, the hydrogen consumption was plotted versus time (Fig. 5). The obtained diagrams indicate clearly that the internal diffusion is more and more limiting with the increase in particle size. But the specific hydrogenation rate is not increased farther for particles under 50 μm in diameter, proving that the internal diffusion is a fortiori not limiting for the kinetic studies performed with particles of 17 μm.

Background of the Kinetic Equations

Our kinetic models were based on the Langmuir–Hinshelwood formalism. Different steps are involved in a catalytic transformation such as adsorption of the reactants, reaction on the active sites at the catalyst surface and desorption of the products. We supposed successively that each of these steps was the rate-limiting step. The competitive adsorption of the organic species and hydrogen, involving only one type of catalytic site, as well as a noncompetitive one, involving two different types of sites, were also considered. We also took into account the possibility of being dissociative or nondissociative for the adsorption of hydrogen.

Finally, 16 models were written, and for each of these models it was supposed that the five reactions of the scheme presented in Fig. 1 were following the same Langmuir–Hinshelwood mechanism. A first selection was based on the examination of Figs. 6 and 7 that show a nearly zero-order dependence with respect to the initial acetophenone concentration, and a varying order (from one to zero) with respect to hydrogen pressure. Only the four models which suppose that the reaction at the catalytic surface is the rate-limiting step are able to predict such dependences. At this stage, a more sophisticated analysis of the results based on the complete kinetic curve is required in order to discriminate between a competitive or noncompetitive adsorption of the species and a dissociative or nondissociative adsorption of hydrogen.

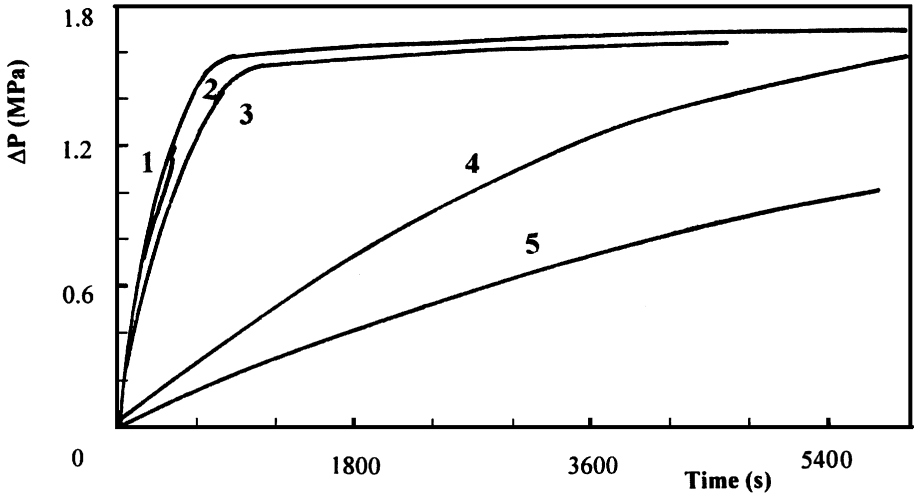

FIG. 5. Hydrogen pressure drop in the storage vessel versus time: Influence of the particle size. $P_{H_2} = 2.5$ MPa, $T = 353$ K, $m_{cata} = 1$ g, and $C^{\circ}_{AC} = 0.6$ mol $\cdot$ l^{-1} (particle diameter d_p being respectively equal to 17, 50, 100, 500, and 3370 μm for curves 1, 2, 3, 4, and 5).

Kinetic Equations

Mass balances corresponding to the four remaining models representing steps 1, 2, 3, 4, 5 of the reaction scheme (Fig. 1) with respective rates r_1, r_2, r_3, r_4, r_5 are written as

$$\frac{dAC}{dt} = (-r_1 - r_2) * \frac{m_{cata}}{V_1}, \qquad t \text{ is time};$$

$$\frac{dPE}{dt} = (r_1 - r_4 - r_5) * \frac{m_{cata}}{V_1}, \qquad P_{H_2} = \text{const};$$

$$\frac{dMCC}{dt} = (r_2 + r_5 - r_3) * \frac{m_{cata}}{V_1}, \qquad C_{H,1} = C^{*}_{H,1} = \frac{P_{H_2}}{He};$$

H_e Henry's const;

$$\frac{dCE}{dt} = (r_3 + r_4)\frac{m_{cata}}{V_1};$$

$$\frac{dn_{H_2}}{dt} = m_{cata}(r_1 + 3r_2 + r_3 + 3r_4 + 2r_5).$$

The rates are (k_i rate constants and K_i adsorption constants):

$$r_1 = k_1 K_{AC} AC * X, \qquad r_2 = k_2 K_{AC} AC * X,$$

$$r_3 = k_3 K_{MCC} MCC * X, \qquad r_4 = k_4 K_{PE} PE * X,$$

$$r_5 = k_5 K_{PE} PE * X.$$

In the case where the mechanism is noncompetitive and nondissociative $X = \alpha$, noncompetitive and dissociative $X = \beta$, competitive and nondissociative $X = \gamma$, competitive and dissociative $X = \delta$ with:

$$\alpha = \frac{1}{(1 + K_{AC}AC + K_{PE}PE + K_{MCC}MCC + K_{CE}CE)} * \frac{K_{H_2}P_{H_2}}{(1 + K_{H_2}P_{H_2})}$$

$$\beta = \frac{1}{(1 + K_{AC}AC + K_{PE}PE + K_{MCC}MCC + K_{CE}CE)} * \frac{\sqrt{K_H P_{H_2}}}{(1 + \sqrt{K_H P_{H_2}})}$$

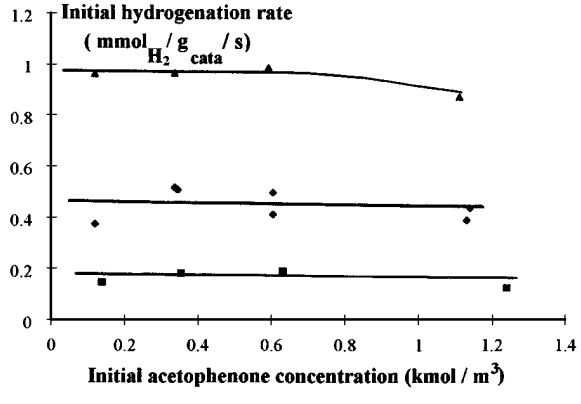

FIG. 6. Initial hydrogenation rate as a function of initial acetophenone concentration: $P_{hé} = 2.5$ MPa, (■) $T = 333$ K, (◆) $T = 353$ K, and (▲) $T = 373$ K.

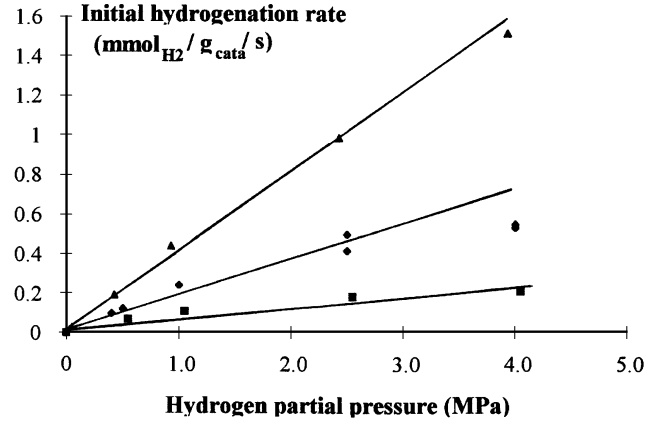

FIG. 7. Initial hydrogenation rate as a function of hydrogen pressure: (■) $T = 333$ K, (◆) $T = 353$ K, and (▲) $T = 373$ K.

$$\gamma = \frac{K_{H_2}P_{H_2}}{\left(1 + K_{AC}AC + K_{PE}PE + K_{MCC}MCC + K_{CE}CE + K_{H_2}P_{H_2}\right)^2}$$

$$\delta = \frac{\sqrt{K_H P_{H_2}}}{\left(1 + K_{AC}AC + K_{PE}PE + K_{MCC}MCC + K_{CE}CE + \sqrt{K_H P_{H_2}}\right)^2}.$$

Optimization of the Kinetic Parameters

The model discrimination and parameter optimization were carried out using a commercial dynamic simulation software (MKF, Cheminform, Saint Petersbourg, Russia). The nonlinear differential equation systems were solved following an iterative method based on the linearisation of the equations. Parameter optimization was performed using the algorithm of the Simplex, based on the minimisation of the best-fit function value, defined as

$$\Phi_i = \frac{\sum_i \left(Y_i^c - Y_i^{exp}\right)^2}{\left(Y_i^{max}\text{error}\right)^2} * \frac{100}{N_{pts}},$$

where Y_i^c is the calculated response value, Y_i^{exp} is the experimental value, and Y_i^{max} is the maximum experimental value. The term "error" is the relative error on the experimental value Y_i^{max} (in our case, the error was fixed at 0.05, the value being representative of the chromatographic error). N_{pts} is the number of points considered for the optimization. A statistical analysis was systematically performed and the confidence intervals of each parameter were calculated.

Results of the Optimization

First of all, the influence of the adsorption constants values on the optimization results was studied for the competitive as well as for the noncompetitive models. In each case, the adsorption constants of the organic species were found to be high (>50 liter $\cdot$ mol^{-1}); the sum $\sum_i K_i C_i$ had to be much greater than one in order to predict the zero order with respect to the acetophenone initial concentration. This fact corresponds to a situation where all of the catalytic sites are occupied by the species, which is quite commonly encountered in the literature (17–19). It was also found that the adsorption constants could not be accurately determined; multiplying each of them by a constant factor gave the same set of optimized kinetic constants and an identical minimum value for the best-fit function. A similar result had already been found by (13), (15), and (33), indicating that only the adsorption constant ratios could be optimized with good precision. The models were then rewritten, introducing the adsorption constant ratios. $Q_i = K_i/K_{PE} \cdot K_{PE}$ was arbitrarily fixed at a value of 100 liter $\cdot$ mol^{-1} and it was checked, *a posteriori*, that our optimization results were not influenced by this value. For a temperature of 353 K, Φ_i—the minimal best-fit function value—amounted to 341 and 351, respectively, for a competitive and noncompetitive dissociative adsorption, but 216 (competitive) and 121 (noncompetitive) for nondissociative adsorption.

Either with the noncompetitive model or the competitive one, a dissociative adsorption of hydrogen did not provide a good fit of the experimental data, the effects of hydrogen pressure being not conveniently represented. At low pressure, $\sqrt{K_H P_{H_2}}$ becomes much smaller than one and the dissociative models predict rates proportional to $\sqrt{K_H P_{H_2}}$ and consequently a 0.5 order dependence with hydrogen pressure which is not in good agreement with the experimental observations (first order at low pressure). Only the nondissociative models provided a good representation of the hydrogen pressure effects. Considering all the data, the noncompetitive model provided the best fit ($\Phi_i = 121$ instead of 216 for the competitive one). Similar computations performed at 333 and at 373 K led to the same model. Activation energies and hydrogen adsorption heat were evaluated, neglecting the effect of temperature on the adsorption constants ratios.

In conclusion, the intrinsic kinetics of acetophenone hydrogenation is well represented by a noncompetitive and nondissociative model, in our range of operating conditions. Table 1 gives the optimum values of the kinetic parameters and their standard deviation and Fig. 8 shows the good agreement between typical experimental concentration profiles and the selected model.

TABLE 1

The Values of the Kinetic Parameters

$\ln k_1^\circ$ (k_1° in mol $\cdot$ kg^{-1} $\cdot$ s^{-1})	26.98 ± 0.01	E_1 (kJ $\cdot$ mol^{-1})	79.65 ± 0.17
$\ln k_2^\circ$ (k_2° in mol $\cdot$ kg^{-1} $\cdot$ s^{-1})	25.41 ± 0.17	E_2 (kJ $\cdot$ mol^{-1})	80.79 ± 2.58
$\ln k_3^\circ$ (k_3° in mol $\cdot$ kg^{-1} $\cdot$ s^{-1})	20.16 ± 0.29	E_3 (kJ $\cdot$ mol^{-1})	69.47 ± 0.89
$\ln k_4^\circ$ (k_4° in mol $\cdot$ kg^{-1} $\cdot$ s^{-1})	27.77 ± 0.38	E_4 (kJ $\cdot$ mol^{-1})	84.62 ± 1.02
$\ln k_5^\circ$ (k_5° in mol $\cdot$ kg^{-1} $\cdot$ s^{-1})	30.79 ± 1.08	E_5 (kJ $\cdot$ mol^{-1})	100.26 ± 3.27
$K_{H_2}^\circ$ (MPa^{-1})	$9.97.10^{-9} \pm 0.02.10^{-9}$	ΔH_H (kJ $\cdot$ mol^{-1})	-49.51 ± 0.1
Q_{AC} (−)	1.68	Q_{MCC} (−)	0.63
K_{PE} (m^3 $\cdot$ kmol^{-1})	100	Q_{CE} (−)	$5, 7.10^{-2}$

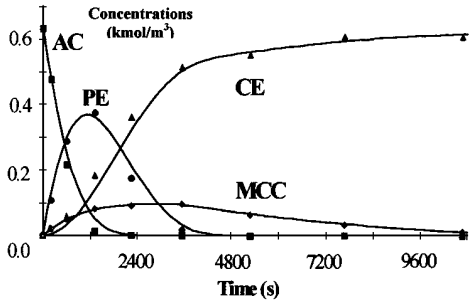

FIG. 8. Experimental and simulated profiles: hydrogenation of acetophenone at T = 333 K, under 2.55 MPa hydrogen pressure and for $[C^{\circ}_{AC}] = 0.631$ mol · l^{-1}.

Discussion

The first point to be discussed is the validity of the selected model. When referring to the few kinetics studies on the hydrogenation of acetophenone, even if the competitive model is often preferred in the case of the selective hydrogenation of acetophenone into phenyl 1-ethanol (7, 14). The noncompetitive model is also proposed (20), in the case of a complex reaction scheme involving the hydrogenation of the aromatic ring as well as the ketone function. It is obvious that the nature of the unsaturated function has a drastic influence on the adsorbates behaviour. When the reaction involves the hydrogenation of a double bond, or of a carbonyle in a linear molecule, the proposed model often considers the competitive adsorption of the species with hydrogen (21–25). But noncompetitive models seem to better represent the hydrogenation of the aromatic ring (17, 19, 26–28). This observation is in good agreement with the fact that the ring is always strongly adsorbed at the catalyst surface (26). Recently a noncompetitive model (33, 34) was proposed for the hydrogenation of several aromatic molecules. Nethertheless, the authors indicate that the hydrocarbon adsorption is probably halfway between competitive and noncompetitive because of the small size of the hydrogen molecule. Concerning hydrogen, dissociatively adsorbed species often coexist with nondissociated ones (bridged and on top species). Among the above references on the hydrogenation of the aromatic ring, some authors consider a nondissociative adsorption of hydrogen. The first to zero-order dependence with hydrogen pressure observed in our case would be in good agreement with the adsorption of at least one molecular hydrogen species, perhaps in minor quantity but presenting a high reactivity. The hydrogenation of the aromatic ring by addition of hydrogen molecular entities has already been demonstrated in the case of the benzene molecule in a gas phase (29). Finally, the noncompetitive and nondissociative model selected for hydrogenation of acetophenone over a Rh/C catalyst is in reasonable agreement with the bibliographic results. Whatever the questions on its unicity, it gives a good formal fit with the intrinsic kinetics of the reaction over a wide range of operating conditions and is useful as such for reactor design.

The second point of this discussion is in relation with the reliability of the estimated parameters. The statistical analysis provides good confidence interval values, indicating that each parameter is accurately obtained. The influence of the K_{PE} value, fixed at 100 liter · mol^{-1} for the study, was evaluated and found to be negligible on the other optimized parameters, as well as on the best-fit function values, as soon as K_{PE} is greater than 50. The adsorption constant ratios are following the expected tendency, increasing with the reactivity of the molecules towards the surface of the metal, due to their degree of unsaturation ($K_{AC} > K_{PE} > K_{MCC} > K_{CE}$). Concerning the value of K_{H_2} expressed in usual units ($K_{H_2} = 4$ liter/mol at T = 353 K), the literature data are so scattered that the value found is in the convenient range (from 10^{-2} liter/mol to 400 liter/mol from (18, 26, 30, 31)). The heat of adsorption optimized for hydrogen ($\Delta H_H = -49.51$ kJ/mol) is slightly larger than those given in the bibliography, but the difference is acceptable (17, 19, 31). The estimated activation energies are also in good agreement with the published results (17–19, 30). Their values are very close to one another for the different steps of the reaction scheme, which agrees fully with the fact that no influence of temperature on the selectivities was observed.

The last point concerns the interaction effects of the species. The selected model and the corresponding set of parameters well represent the intrinsic kinetics of acetophenone hydrogenation; they should also fit the kinetics of hydrogenation of intermediates such as phenyl 1-ethanol and methylcyclohexylketone. To verify this fact, experiments were then performed with pure phenyl 1-ethanol or pure methylcyclohexylketone in the same range of operating conditions. The experimental results were simulated using the noncompetitive and nondissociative model and the parameter values given in Table 1. They are suitable to represent phenyl 1-ethanol hydrogenation (maximum disagreement 10%) but not well adapted to the kinetics of methylcyclohexylketone (68% discrepancy with experimental data). It was also checked that another set of parameters could not provide a good fitting for both hydrogenation of acetophenone and hydrogenation of methylcyclohexylketone. Vice versa, the optimization of kinetic parameters on hydrogenation of intermediates cannot be directly used for hydrogenation of acetophenone because they do not provide the best fit. They can only be used as initial values. Similar limitations had already been observed (15) for hydrogenation of nitriles. The interaction between the adsorbed species are probably not negligible and more sophisticated models, including these effects and accounting for the complexity of the catalytic surface, should be developed.

In conclusion, this study shows the complexity of model discrimination and parameter optimization for a multistep reaction scheme. In the case where a more realistic model would be wanted the adsorbed species lateral interactions could not be neglected and should be taken into account. Nevertheless, the noncompetitive and nondissociative hypotheses selected here to represent the intrinsic kinetics of acetophenone hydrogenation provide a good representation of all the concentration profiles in a batch reactor over a wide range of operating conditions within the interval of experimental precision. In particular this model remains perfectly adapted for reactor calculations.

Kinetics Modelling in a Diffusion Regime

Model Assumptions

The catalyst was purchased as 3.37-mm particles to be used in fixed bed reactors like trickle beds. That is why we needed to study the effects of the particle size on the activity. For this purpose, experiments were performed in a semibatch reactor for different particle sizes. The hydrogen consumption plotted versus time indicates clearly a decrease in activity in function of the particle diameters due to internal diffusion (see Fig. 5). The concentration profiles have also been represented versus time for samples of uniform particle size. They show that selectivities were affected to some extent by intraparticle diffusion limitation: when the particle size was varied from 17 to 3370 μm, the maximum phenyl 1-ethanol yield is altered from 65 to 55%. In order to predict the behaviour of multiphase reactors, wherein internal mass transfer limitations are large, an intraparticle diffusion model was developed using the intrinsic kinetics established above.

Because of the catalyst characteristics described in the experimental part, the large particles ($d_p = 3.37$ mm) were considered as spherical and impregnated with rhodium metal with an "eggshell" distribution. The fraction of the catalyst particles containing metal is called the active fraction (noted F_{active}) and depends on the thickness of the impregnation layer (noted E_{p0}). In this layer, the rate per mass of active catalyst (containing metal) r'_i, is equal to the rate given by the kinetic study r_i (given per total mass of catalyst) divided by F_{active}. Small particles were obtained by crushing and sieving the largest of the commercial catalyst. They were also considered as spherical and it was supposed that only a part of them (equal to F_{active}) contained metal contributing to the reaction, the other part being free of rhodium and totally inactive.

Two models were developed: one being written for the totally active small particle ($d_p \leq 100$ μm) and considering a spherical geometry, and the other for the large particles ($d_p = 3.37$ mm) and considering a plane geometry for the active layer. It was controlled *a posteriori* by electron microscopy that the active layer of the catalyst grains (noted E_p), was always small, compared to the largest diameter d_p, and could be modelled by a plane layer. The sets of equations in Table 2 were solved numerically using an orthogonal collocation method (32) for the mass balance on the solid and a fourth-order Runge–Kutta method for the mass balance on the liquid.

TABLE 2

Set of Equations Solved Numerically

Mass balance on the solid

Small particles ($d_p \leq 100$ μm)

$$\frac{De_{AC}}{r^2}\frac{d}{dr}\left(r^2\frac{d[AC]_s}{dr}\right) = \rho_P\left(r'_1 + r'_2\right)$$

$$\frac{De_{PE}}{r^2}\frac{d}{dr}\left(r^2\frac{d[PE]_s}{dr}\right) = \rho_P\left(-r'_1 + r'_4 + r'_5\right)$$

$$\frac{De_{MCC}}{r^2}\frac{d}{dr}\left(r^2\frac{d[MCC]_s}{dr}\right) = \rho_P\left(-r'_2 - r'_5 + r'_3\right) +$$

$$\frac{De_{CE}}{r^2}\frac{d}{dr}\left(r^2\frac{d[CE]_s}{dr}\right) = \rho_P\left(-r'_3 - r'_4\right)$$

$$\frac{De_{H_2}}{r^2}\frac{d}{dr}\left(r^2\frac{d[H_2]_s}{dr}\right) = \rho_P\left(r'_1 + 3r'_2 + r'_3 + 3r'_4 + 2r'_5\right)$$

$0 < r < d_p/2$

Large particles (d_p=3.37 mm)

$$De_{AC}\frac{d}{dx}\left(\frac{d[AC]_s}{dx}\right) = \rho_P\left(r'_1 + r'_2\right)$$

$$De_{PE}\frac{d}{dx}\left(\frac{d[PE]_s}{dx}\right) = \rho_P\left(-r'_1 + r'_4 + r'_5\right)$$

$$De_{MCC}\frac{d}{dx}\left(\frac{d[MCC]_s}{dx}\right) = \rho_P\left(-r'_2 - r'_5 + r'_3\right)$$

$$De_{CE}\frac{d}{dx}\left(\frac{d[CE]_s}{dx}\right) = \rho_P\left(-r'_3 - r'_4\right)$$

$$De_{H_2}\frac{d}{dx}\left(\frac{d[H_2]_s}{dx}\right) = \rho_P\left(r'_1 + 3r'_2 + r'_3 + 3r'_4 + 2r'_5\right)$$

$0 < x < E_p$

Boundary conditions

Small particles ($d_p \leq 100$ μm)

$r = 0$: $\frac{d[AC]_s}{dr} = 0; \frac{d[PE]_s}{dr} = 0;$

$\frac{d[MCC]_s}{dr} = 0; \frac{d[CE]_s}{dr} = 0; \frac{d[H_2]_s}{dr} = 0$

$r = d_p/2$: $[AC]_s = [AC]_l$; $[PE]_s = [PE]_l$

$[MCC]_s = [MCC]_l$; $[CE]_s = [CE]_l$

$[H_2]_s = [H_2]^*$

Large particles (d_p=3.37 mm)

$x = 0$: $\frac{d[AC]_s}{dx} = 0$; $\frac{d[PE]_s}{dx} = 0$

$\frac{d[MCC]_s}{dx} = 0$; $\frac{d[CE]_s}{dx} = 0$; $\frac{d[H_2]_s}{dx} = 0$

$x = E_p$: $[AC]_s = [AC]_l$; $[PE]_s = [PE]_l$

$[MCC]_s = [MCC]_l$; $[CE]_s = [CE]_l$

$[H_2]_s = [H_2]^*$

Mass balance on the liquid

Small particles ($d_p \leq 100$ μm)

$$\frac{d[AC]_l}{dt} = (-\eta_1 r'^s_1 - \eta_2 r'^s_2)\frac{m_{cata}F_{active}}{V_l}$$

$$\frac{d[PE]_l}{dt} = (\eta_1 r'^s_1 - \eta_4 r'^s_4 - \eta_5 r'^s_5)\frac{m_{cata}F_{active}}{V_l}$$

$$\frac{d[MCC]_l}{dt} = (\eta_2 r'^s_2 + \eta_5 r'^s_5 - \eta_3 r'^s_3)\frac{m_{cata}F_{active}}{V_l}$$

$$\frac{d[CE]_l}{dt} = (\eta_3 r'^s_3 + \eta_4 r'^s_4)\frac{m_{cata}F_{active}}{V_l}$$

$$\eta_i = \frac{\int_0^{dp/2} 4\pi^2 r'_i dr}{\frac{4\pi}{3}\left(\frac{d_p}{2}\right)^3 r'^s_i}; F_{active} = 1 - \frac{\left(\frac{d_p}{2} - E_{p0}\right)^3}{\left(\frac{d_p}{2}\right)^3}$$

Large particles (d_p=3.37 mm)

$$\frac{d[AC]_l}{dt} = (-\eta_1 r'^s_1 - \eta_2 r'^s_2)\frac{m_{cata}F_u}{V_l}$$

$$\frac{d[PE]_l}{dt} = (\eta_1 r'^s_1 - \eta_4 r'^s_4 - \eta_5 r'^s_5)\frac{m_{cata}F_u}{V_l}$$

$$\frac{d[MCC]_l}{dt} = (\eta_2 r'^s_2 + \eta_5 r'^s_5 - \eta_3 r'^s_3)\frac{m_{cata}F_u}{V_l}$$

$$\frac{d[CE]_l}{dt} = (\eta_3 r'^s_3 + \eta_4 r'^s_4)\frac{m_{cata}F_u}{V_l}$$

$$\eta_i = \frac{\int_0^{Ep} r'_i dx}{E_p r'^s_i}; F_u = 1 - \frac{\left(\frac{d_p}{2} - E_p\right)^3}{\left(\frac{d_p}{2}\right)^3}$$

Rate Expressions (mol/kg Active Catalyst/s)

$r'_i = r_i/F_{active}$ with r_i function of the concentrations inside the solid whatever the size of the particle.

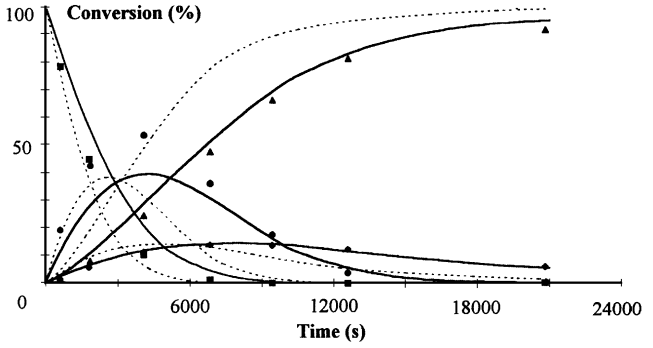

FIG. 9. E_{p0} value effects on the simulations: $d_p = 3{,}37$ mm; $C^{\circ}_{AC} = 0{,}604$ mol · l^{-1}; T = 353 K; $P_{H_2} = 2{,}5$ MPa; $m_{cata} = 1.0$ g; (■) AC; (◆) MCC; (▲) PE; (●) CE; ———. Simulated curve for $E_{p0} = 1000$ μm and ---- $E_{p0} = 300$ μm.

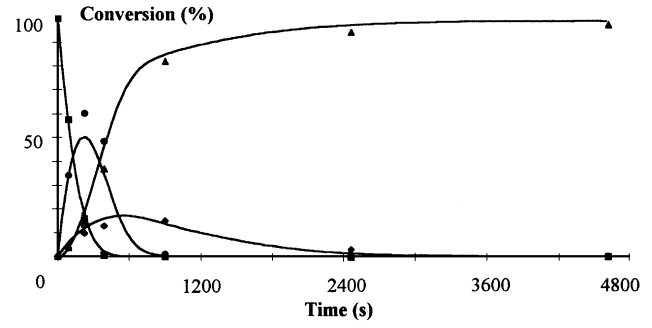

FIG. 10. Comparison of simulated and experimental profiles: $E_{p0} = 1000$ μm; $d_p = 100$ μm; $C^{\circ}_{AC} = 0.604$ mol · l^{-1}; T = 353 K; $P_{H_2} = 2.5$ MPa; $m_{cata} = 1.0$ g; (■) AC; (◆) MCC; (●) PE; (▲) CE; ——— simulation.

Results and Discussion

First of all, the thickness of the impregnation layer E_{p0} was evaluated. Electron microscope diagrams provide only an approximate value of E_{p0} because, on the one hand, the particles used are not perfectly spherical as considered in the model and, on the other hand, very small and highly active rhodium crystallites can possibly be present at the center of the catalyst but are not detected by the electron micrographs. A good estimation of E_{p0} value being essential for the rate and effectiveness factors computations, experiments using different particle sizes were simulated for several E_{p0} values. For particle diameters smaller than 100 μm, the simulations were found to be insensitive to the E_{p0} value and the concentration profiles were as well represented with $E_{p0} = 300$ μm as with $E_{p0} = 1000$ μm. Conversely, simulations were found to be highly sensitive to the E_{p0} value in the case of large particles as is shown in Fig. 9. This result seems logical since the intraparticle diffusion is highly limiting for this particle size. With $E_{p0} = 1000$ μm providing the best fit to all our experimental datas, this value was used for the whole study.

Experiments performed with different particle sizes were simulated and the results compared to the experimental data. In order to confirm that intraparticle diffusion was not limiting for the kinetic study, every experiment performed with particles of 17 μm diameter was simulated and the effectiveness factors were calculated. They were found to be equal to 1 ± 0.05 in every case, proving the kinetic regime and in good agreement with the experimental results on the influence of the particle size between 17 and 50 μm (see Fig. 5). For small particles ($d_p = 50$ μm and $d_p = 100$ μm), simulated profiles were found to be in good agreement with the experimental ones. As an example, Figs. 10 and 11 show the results obtained for $d_p = 100$ μm. Only the maximum obtained for the phenyl 1-ethanol profile is slightly underestimated by the model, but the difference remains acceptable.

Effectiveness factors η_1 and η_2 are always lower than one varying from 0.9 to 0.78 for $d_p = 50$ μm and from 0.7 to 0.45 for $d_p = 100$ μm, as long as acetophenone concentration is not equal to zero. These results indicate clearly the increasing intraparticle diffusion limitation with the particle size. η_3 , η_4, and η_5 (related to the reactions of the intermediates PE and MCC) are greater than one at the beginning and decrease later to values lower or equal to one. Intermediates are formed inside the pores of the catalyst. Their concentrations are, at the beginning of the experiment, higher inside the particle than at the surface, leading to effectiveness factors greater than one. The more limiting the internal diffusion, the higher is this overconcentration. When the acetophenone disappears, the intermediate formation slows down and their profiles inside the particle become concave. Then, the effectiveness factors decrease to values lower than one.

For large particles, the computed effectiveness factors η_1 and η_2 (Fig. 12) were very low (from 0.07 to 0.045), which is consistent with the observed hydrogenation rates. η_3, η_4, and η_5 are greater than one at the beginning and decrease rapidly to values lower than one (0.05 to 0.15), indicating the strong limitation by intraparticle diffusion.

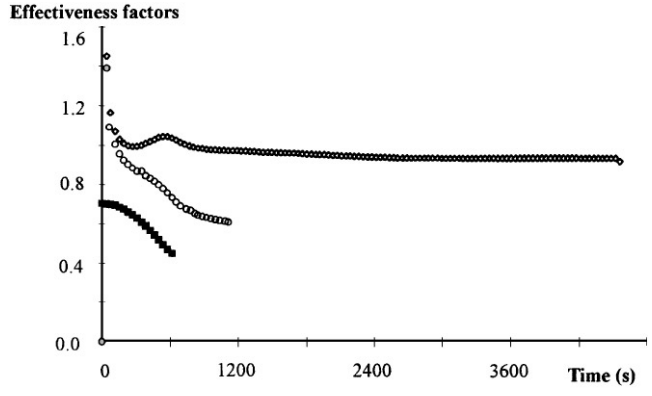

FIG. 11. Effectiveness factors (■) $\eta_1 - \eta_2$; (◇) η_3, and (○) $\eta_4 - \eta_5$ for $E_{p0} = 1000$ μm; $d_p = 100$ μm; $C^{\circ}_{AC} = 0.604$ mol · l^{-1}; T = 353 K; $P_{H_2} = 2.5$ MPa; $m_{cata} = 1.0$ g.

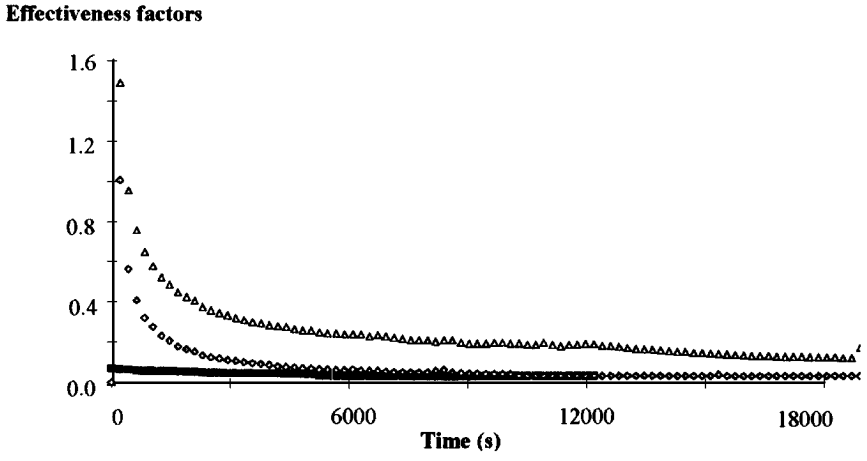

FIG. 12. Effectiveness factors (■) $\eta_1-\eta_2$; (△) η_3, and (◇) $\eta_4-\eta_5$ for $E_{p0}=1000\ \mu$m; $d_p=3370\ \mu$m; $C^{\circ}_{AC}=0.604\ \text{mol}\cdot\text{l}^{-1}$; T = 353 K; $P_{H_2}=2.5$ MPa; $m_{cata}=1.0$ g.

Simulated profiles were also found to be in good agreement with the experiments despite the fact that the phenyl 1-ethanol concentration is once again slightly underestimated (25%). One way to improve the fit of the PE profile for all the particle sizes is to adjust the value of the adsorption constants ratio Q_{AC} by increasing it from $Q_{AC}=1.67$ (given by the intrinsic kinetics study) to $Q_{AC}=4$ (Fig. 13). This adjustement can probably be considered as a consequence of the species interaction effect. As was previously observed during the kinetics study, some parameter values such as the adsorption constants could possibly be affected by the concentration of the species in the solution. The interaction between adsorbed species are probably not negligible and this phenomenon is not accounted for in the used Langmuir–Hinshelwood equations used. Nevertheless, by adjusting one of the adsorption constant ratios, the proposed intraparticle diffusion models provide a very good representation of the experimental data in a wide range of particle sizes in terms of activity and selectivity. They will be helpful to predict the performances of multiphase reactors using large particles such as fixed beds.

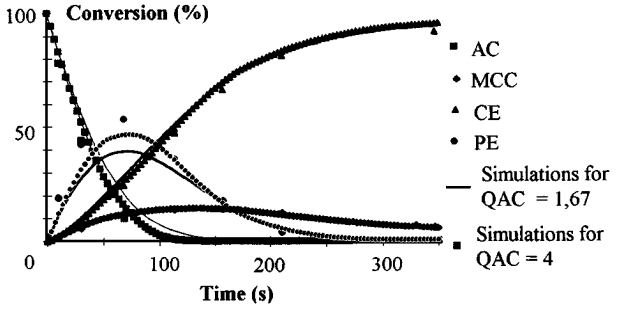

FIG. 13. Experimental and simulated concentration profiles in semi-batch reactor for $d_p=3370\ \mu$m; $C^{\circ}_{AC}=0.604\ \text{mol}\cdot\text{l}^{-1}$; T = 353 K; $P_{H_2}=2.5$ MPa; $m_{cata}=1.0$ g; (■) AC; (◆) MCC; (▲) CE; (●) PE; (■) simulations with $Q_{ac}=4$; ——— simulations with $Q_{ac}=1.67$.

GENERAL CONCLUSION

The kinetics of acetophenone hydrogenation on a Rh/C catalyst was experimentally studied in the conditions of chemical and diffusion regimes. The discrimination between different possible reaction mechanisms and the parameter optimization were made by means of a computer program, especially in the case of diffusion limiting transfer. This is useful for the modelling of fixed bed reactors where large catalyst particles are used. A noncompetitive and nondissociative model based on a Langmuir–Hinshelwood type surface reaction was compared to the experiments. In this way it was possible to obtain a mathematical representation of the experimental results within the limits of experimental precision. Nevertheless, some hydrogenation experiments on pure intermediates of the reaction, in particular the strongly adsorbed phenyl-1 ethanol, showed that this model, neglecting the adsorbed species interaction effects, was not sophisticated enough to be universal.

REFERENCES

1. Mushenko, D. V., Lebedeva, E. G., Khimich, V. P., Chagina, V. S., and Barinov, N. S., *Zh. Prikl. Khim.* **39**, 2766 (1966).
2. Mushenko, D. V., Lebedeva, E. G., Chagina, V. S., Khimich, V. P., and Barinov, N. S., *Zh. Prikl. Khim.* **39**, 2769 (1966).
3. Barinov, N. S., Mushenko, D. V., and Lebedeva, E. G., *Zh. Prikl. Khim.* **42**, 2398 (1969).
4. Barinov, N. S., Lebedeva, E. G., and Mushenko, D. V., *Zh. Prikl. Khim.* **42**, 2613 (1969).
5. Barinov, N. S., and Mushenko, D. V., *Zh. Prikl. Khim.* **46**, 940 (1973).
6. Barinov, N. S., and Mushenko, D. V., *Izvest. Otdel. Khim. Nauk.* **6**, 507 (1973).
7. Geneste, P., and Lozano, Y., *C.R. Acad. Sc. Paris C* **280**, 1137 (1975).
8. Masson, J., Cividino, P., Bonnier, J. M., and Fouilloux, P., *Heterogeneous Catalysis and Fine Chemicals II* **59**, 245 (1991).
9. Mushenko, D. V., Barinov, N. S., and Lebedeva, E. G., *Zh. Organ. Khim.* **7**, 314 (1971).

10. Csomontanyi, G., Netta, M., and Balmez, M., *Revue roumaine de chimie* **18**, 1367 (1973).
11. Serebryakov, B. R., Smirnova, N. A., and Garbuzov, V. G., *Azerb. Khim. Zh.* **6**, 135 (1977).
12. Del Amo, F. B., *Ingenieria Quimica* (Madrid) **23**, 115 (1991).
13. Cerveny, L., Dobrovolna, Z., Belohlav, Z., and Kluson, P., *Collect. Czech. Chem. Commun.* **61**, 764 (1996).
14. Ziyatdinov, A. S., Stepanenko, V. V., Chernykh, I. S., Leonova, E. B., Pisarenko, V. N., and Kafarov, V. V., *Zh. Priklad. Khim.* **61**, 565 (1988).
15. Joly-Vuillemin, C., Gavroy, D., Cordier, G., De Bellefon, C., and Delmas, H., *Chem. Eng. Sci.* **49**, 4839 (1994).
16. Wilke, C. R., and Chang, P., *AIChE. J.* **1**, 264 (1955).
17. Zwicky, J. J., and Gut, G., *Chem. Eng. Sci.* **33**, 1363 (1978).
18. Gut, G., Kosinka, J., Prabucki, A., and Schuerch, A., *Chem. Eng. Sci.* **34**, 1051 (1979).
19. Turek, F., Geike, R., and Lange, R., *Chem. Eng. Processes.* **20**, 213 (1986).
20. Smirnova, N. A., Adamyan, V. L., Edigavora, E. I., and Likhushkin, I. A., *Azerb. Khim. Zh.* **4**, 44 (1987).
21. Kishida, S., and Teranishi, S., *J. Catal.* **12**, 90 (1968).
22. Lemcoff, N. O., *J. Catal.* **46**, 356 (1977).
23. Chaudhari, R. V., Parande, M. J., Ramachandran, P. A., Brahme, P. H., Vadgaonkar, H. G., and Jaganathan, R., *AIChE. J.* **31**, 1891 (1985).
24. Chaudhari, R. V., Jaganathan, R., Kolhe, S., Emig, G., and Hofmann, H., *Chem. Eng. Sci.* **41**, 3073 (1986).
25. Smedler, G., *Can. J. Chem. Eng.* **67**, 51 (1989).
26. Kawakami, K., Ura, K., and Kusunoki, K., *J. Chem. Eng. Japan* **9**, 392 (1976).
27. Broderick, D. H., and Gates, B. C., *AIChE J.* **27**, 663 (1981).
28. Kut, O. M., Yücelen, F., and Gut, G., *J. Chem. Tech. Biotechnol.* **39**, 107 (1987).
29. Mirodatos, C., Dalmon, J. A., and Martin, G. A., *J. Catal.* **105**, 405 (1987).
30. Turek, F., Chakrabarti, R. K., Lange, R., Geike, R., and Flock, W., *Chem. Eng. Sci.* **38**, 275 (1983).
31. Gupta, A. K., Bhattacharyya, and Saraf, S. K., *Indian J. Technol.* **23**, 184 (1985).
32. Villadsen, J. V., and Stewart, W. E., *Chem. Eng. Sci.* **22**, 1483 (1976).
33. Toppinen, S., Salmi, T., Rantaquiä, T. K., and Aittanaa, J., *Ind. Eng. Chem. Res.* **36**, 2101 (1997).
34. Salmi, T., Toppinen, S., Rantaquiä, T. K., and Aittanaa, J., *in* "Proc. First European Congress on Chemical Engineering, Florence, Italy, May 4–7, 1997," p. 2947.